Agricultural and Forest Meteorology 296 (2021) 108217

Contents lists available at ScienceDirect

Agricultural and Forest Meteorology

journal homepage: www.elsevier.com/locate/agrformet

Cross-scale evaluation of dynamic crop growth in WRF and Noah-MP-Crop

Trevor F. Partridge[a,*], Jonathan M. Winter[b,a], Anthony D. Kendall[c], David W. Hyndman[c]

[a] Department of Earth Sciences, Dartmouth College, Hanover, NH, USA
[b] Department of Geography, Dartmouth College, Hanover, NH, USA
[c] Department of Earth and Environmental Sciences, Michigan State University, East Lansing, MI

ARTICLE INFO

Keywords:
Regional climate model
Agriculture
Crop model
Land-atmosphere interactions

ABSTRACT

Accurately representing croplands in climate models is important for simulating water and energy fluxes between the land and atmosphere, as well as evaluating the impacts of climate change on agriculture. The recent integration of dynamic crop growth in the Noah land surface model with multiparameterization (Noah-MP-Crop) has the potential to substantially advance Earth system modeling and is included in the latest release of the Weather Research and Forecasting (WRF) regional climate model. The addition of dynamic crop growth to WRF provides a unique opportunity to simultaneously evaluate biases associated with a crop model coupled to a regional climate model and address outstanding questions regarding the role of agroecosystems in modulating regional climate. Here, we analyze dynamic crop growth in WRF across three simulated spatial scales (25km, 5km, and 1km) for growing seasons with precipitation above (2010), below (2012), and approximately equal (2015) to the seasonal average. Including dynamic crop growth in WRF significantly reduces biases in simulated leaf area index over croplands in the central U.S. relative to observations. However, there is no substantial difference in calculated daily evapotranspiration, average growing season temperature, or total growing season precipitation between WRF simulations with dynamic crops (WRF-Crop) compared to the dynamic vegetation module without crops (WRF-DV). Simulated corn (soy) mean absolute error (MAE), as a percentage of observed annual average yield, ranges from 24.7% -101% (28.1% - 109%) depending on year and spatial resolution, with the most significant biases in highly irrigated counties. Forcing Noah-MP-Crop with observed climate substantially reduces the range of corn (soy) yield MAE to 9.5% - 55.1% (15.0% - 37.5). Increased model resolution consistently leads to lower corn and soy yield estimates within WRF-Crop.

1. Introduction

Climate and agriculture are inherently linked. Large-scale transitions from natural landscapes and ecosystems to heavily managed croplands and pasturelands, along with the expansion of irrigation over the last 60 years, have significantly modified hydrologic and carbon cycles, altered land-atmosphere interactions, and impacted local, regional, and global climate (Foley et al., 2005; Pielke et al., 1998; Spera et al., 2020; Thiery et al., 2020). Today, approximately 35% of global land area is devoted to growing food (World Bank, 2020) and nearly 70% of all freshwater withdrawals are used to irrigate crops and pasturelands (FAO, 2017; Siebert et al., 2010). In the contiguous United States roughly 19% of the land area is devoted to growing crops and irrigation accounted for 42% of total freshwater withdrawals in 2015 (Dieter et al., 2018). Rising temperatures, altered precipitation patterns, and more frequent and intense extreme weather events due to climate change are already impacting agriculture, and will continue to do so in the future (Lobell, et al., 2011; Rosenzweig & Parry, 1994; Wuebbles et al., 2014). Agriculture is a significant driver of climate change, accounting for roughly 30% of total global anthropogenic greenhouse gas emissions and nearly 60% of non-CO_2 emissions (Tubiello et al., 2014). Understanding feedbacks between agricultural systems and climate is paramount to

Abbreviations: LAI, Leaf Area Index; ET, Evapotranspiration; GDDs, Growing Degree Days; WRF, Weather Research and Forecasting model; WRF-Crop, WRF simulations using Noah-MP with dynamic crop growth; WRF-DV, WRF simulations using Noah-MP without dynamic crop growth but with dynamic vegetation; Noah-MP, Noah land surface model with multiparameterization; HRLDAS, High-Resolution Land Data Assimilation System; HRLDAS-Crop, HRLDAS simulations using Noah-MP with dynamic crop growth; NLDAS, North American Land Data Assimilation System; CDL, Cropland Data Layer; MAE, Mean Absolute Error.

* Corresponding author
E-mail addresses: trevor.f.partridge.gr@dartmouth.edu (T.F. Partridge), jonathan.m.winter@dartmouth.edu (J.M. Winter), kendal30@msu.edu (A.D. Kendall), hyndman@msu.edu (D.W. Hyndman).

https://doi.org/10.1016/j.agrformet.2020.108217
Received 19 June 2020; Received in revised form 8 September 2020; Accepted 6 October 2020
Available online 4 November 2020
0168-1923/

developing effective adaptation and mitigation strategies (McDermid, et al., 2017).

Converting natural landscapes to croplands through deforestation or tilling native vegetation modifies the surface albedo, alters latent and sensible heat fluxes, perturbs the boundary layer, and impacts regional temperature and precipitation patterns (Adegoke et al., 2007; Bonan, 2008; Pielke et al., 1998). Management of croplands, including irrigation and planting practices, can also have notable impacts on climate. Irrigation can directly link groundwater reservoirs to the surface, which can enhance evapotranspiration (ET) over irrigated land (Uddin, et al., 2013). Increased ET can reduce local and regional temperatures through increased evaporative cooling (Kueppers, et al., 2007; Puma & Cook, 2010), and has been shown to increase local and regional precipitation as a result of enhanced precipitable water and convective available potential energy (Pei et al., 2016). Irrigation has also been linked to warmer nighttime temperatures as a result of an increased heat storage capacity of wetter soils (Chen & Jeong, 2018) and increased net surface radiation due to a lower soil albedo and enhanced absorption of long-wave radiation by increased water vapor in the upper atmosphere (Boucher et al., 2004; Otterman, 1977). Increased plant density in both rainfed and irrigated croplands has also been shown to enhance local ET, resulting in a regional cooling effect. These combined effects may contribute to the "warming hole" over the U.S. (Alter, et al., 2018; Mueller et al., 2016; Nikiel & Eltahir, 2019; Partridge et al., 2018), which has in turn likely boosted agricultural productivity in the region (Partridge et al., 2019). While it is clear that agricultural practices modulate climate, many of the models used to explore the feedbacks between climate and croplands use a prescribed crop LAI or dynamically simulate crops as generic grasses, both of which could result in significant biases as crops are known to respond to weather and climate variations through both natural and managed processes (Lu, et al., 2015).

In recent years, several studies have simulated dynamic crop growth in climate and land surface models (Drewniak et al., 2013; Kucharik, 2003; Levis et al., 2012; Osborne et al., 2009; Lu et al., 2015; Liu et al., 2016). Osborne et al. (2009) found that including dynamic crop growth in a global climate model increased growing season temperature variability in the tropics by up to 40% during dry years. Levis et al. (2012) integrated corn, soy, and cereal crops into the Community Earth System Model (CESM1) and found improved representations of surface heat fluxes due to more realistic seasonal LAI patterns and net ecosystem exchange. The 4th version of the Community Land Model (CLM4), which includes dynamic crop growth and irrigation within WRF (WRF-CLM4-crop), has been evaluated against observations (Lu et al., 2015) and compared to simulations with a prescribed LAI (Harding et al., 2015). WRF-CLM4-crop overestimates LAI and growing season length, but dynamic crop growth improves interannual variability of LAI relative to prescribed LAI values. Simulating irrigation improves temperature, soil moisture, and surface energy flux biases compared to observations (Lu et al., 2015), but the effect of irrigation on precipitation in WRF-CLM4-crop is dependent on dynamic crop growth. Simulations with dynamic crop growth showed a significant correlation between precipitation and water used for irrigation, while those with prescribed crop growth did not (Harding et al., 2015).

Incorporating dynamic crop growth in climate models also expands our understanding of the feedbacks between weather variability, climate change, and agricultural productivity, which is essential for short- and long-term yield projections. The integration of dynamic crop growth in land surface models is often based on simplified representations from traditional biophysical crop models, which simulate daily plant growth as a function of temperature, precipitation, environmental stress, and management. Traditional biophysical crop models require large amounts of input data such as cultivar type, planting and harvest dates, and fertilizer application rates. This makes them cumbersome to directly couple with climate models over data-limited areas or for projections, as management practices are likely to change in the future. However, uncoupled traditional biophysical crops models do not capture feedbacks between crops and the atmosphere, which can have important implications for yield (Thiery et al., 2017).

Dynamic crop growth was recently integrated into the Noah land surface model with multiparameterization (Noah-MP-Crop; Niu et al., 2011; Liu et al., 2016) and implemented in version 3.7 of the Weather Research and Forecasting (WRF; Skamarock et al., 2019) regional climate model. Noah-MP-Crop simulates the growth of both corn (*Zea mays)* and soy (*Glycine max)* using plant growth stages determined by accumulating growing degree days (GDDs), or the accumulated daily average temperature above a threshold. Each plant growth stage has a unique set of carbohydrate allocation coefficients that dictate carbon assimilation (from photosynthesis) and loss (from respiration, turnover, and senescence) for each carbon pool within the plant (roots, stem, leaves, and grain). Noah-MP-Crop has been shown to reasonably capture LAI, surface latent and sensible heat fluxes, and above ground biomass for both corn and soy relative to observations when forced with meteorological data from Ameriflux eddy covariance towers in Bondville, IL and Meade, NE (Liu et al., 2016). Zhang et al. (2020) recently evaluated regional simulations of Noah-MP-Crop across the central U.S. with and without the irrigation scheme developed by Xu et al. (2019). They found that including irrigation and spatially varying planting and harvest dates significantly reduced yield biases.

Here, we evaluate Noah-MP with dynamic crop growth coupled to WRF by comparing simulated LAI, ET, temperature, precipitation, and yield to observations. To the best of our knowledge, Noah-MP-Crop has yet to be assessed in dynamically coupled simulations with WRF. We run three triple-nested WRF simulations over the central U.S. (Fig. 1) for 2010, 2012, and 2015; these correspond with a wetter than average year, a drought year, and a year with approximately normal precipitation for the central U.S. The first set of simulations uses the pre-existing dynamic vegetation module within Noah-MP (hereafter WRF-DV), the second set uses dynamic crop growth within Noah-MP (hereafter WRF-Crop), and the third set uses an offline version of Noah-MP-Crop run within the High Resolution Land Data Assimilation System (hereafter HRLDAS-Crop; Chen et al., 2007) to isolate errors associated with simulated climate. Our simulations do not account for irrigation on the landscape.

2. Data and Methods

We evaluated the performance of WRF-Crop relative to observed climate, LAI, ET, and crop yield data. We used observed temperature and precipitation from Daymet, Leaf Area Index (LAI) and estimated ET from both the MODerate Resolution Imaging Spectroradiometer (MODIS) satellite and the eddy covariance flux tower at the Brooks experimental field site in Ames Iowa, and reported county-level corn and soy yield data from USDA NASS.

Daymet is a 1km gridded daily observational product covering North America from 1980 to present available from the Oak Ridge National Laboratory Distributed Active Archive Center (Thornton et al., 2018). This data product was developed using ground observations from the Global Historical Climatology Network-Daily dataset, and has been widely used in regional climate model evaluation analyses (e.g. Bukovsky & Karoly, 2011; Huang et al., 2020).

For evapotranspiration (ET), we used the MOD15A2H 8-day, 500m global LAI product (Myneni et al., 2015), and the MOD16 8-day 500m global ET product (Running et al., 2017), which are both derived from the MODIS instrument aboard NASA's Terra satellite. Both MODIS datasets were acquired from the USGS AppEARS data portal. The MOD16 ET product combines daily meteorological reanalysis data with land cover estimates, albedo, and vegetation dynamics from MODIS using an algorithm developed by Mu et al. (2007, 2011) based on the Penman-Monteith equation. MOD16 ET has been evaluated for biomes across the globe, and is generally well correlated with independent estimates of ET from observations and models (Ramoelo et al., 2014; Sun et al., 2007; Velpuri et al., 2013). Data from the US-Br-1 fluxtower was

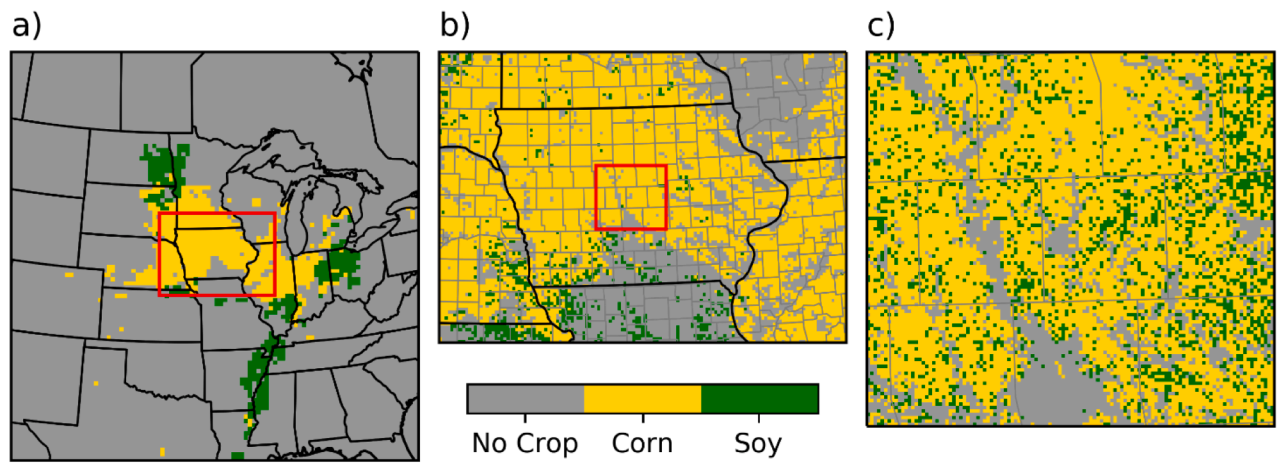

Figure 1. WRF nested domains and crop category within each domain. The spatial resolution of domain 1 is 25 km (a), domain 2 is 5 km (b), and domain 3 is 1 km (c). Crop category is determined by the dominant crop type in each grid cell.

downloaded from the Ameriflux website (ameriflux.lbl.gov). The Brooks Field site is planted in a corn-soy rotation with management practices similar to agricultural sites across the central U.S.

2.1. Model Configuration

We used the Weather Research and Forecasting (WRF) regional climate model version 4.0.1 (Skamarock et al., 2019) to run one-way triple nested simulations over the central United States. We simulated climate during 2010, 2012, and 2015, to examine years with growing season precipitation above, below, and approximately equal to the long-term average, respectively. We ran each simulation for the full year, but only analyzed results over the growing season (approximately May–September) reserving January through April for model spin-up. The model domain (shown in Fig. 1) is centered over Iowa with spatial resolution increasing from 25 km (D1) to 5 km (D2) to 1 km (D3). We utilized an adaptive time step, which has been shown to improve model efficiency without affecting model bias (Hutchinson, 2007). For boundary and initial conditions, we used six-hourly data from the European Centre for Medium Range Weather Forecast Reanalysis-Interim (ERA-I; Berrisford et al., 2011). Physics parameterization schemes include: Kain-Fritsch for convective rainfall, WSM3 microphysics, Yonsei University planetary boundary layer, Dudhia shortwave radiation, and RRTM longwave radiation. We allowed WRF to explicitly resolve convection within the 1 km domain (Pieri et al., 2015). WRF does come with a suggested physics package for the U.S., however we found that a component of that physics package, the Thompson microphysics scheme, was not compatible with dynamic crop growth in Noah-MP. We ran three simulations for each year: one using Noah-MP with dynamic crop growth (WRF-Crop), the second using Noah-MP without dynamic crops but with dynamic vegetation (WRF-DV), and the third decoupled from WRF using the High-Resolution Land Data Assimilation System (HRLDAS-Crop; Chen et al., 2007). For HRLDAS-Crop simulations, we used hourly data from the North American Land Data Assimilation System (NLDAS; Xia et al., 2012) instead of ERA-I as forcing data. NLDAS combines climate and land surface observations from multiple sources with reanalysis products to create a temporally and spatially consistent dataset at 1/8° (Luo et al., 2003). We chose to force HRLDAS-Crop with NLDAS instead of ERA-I due to its increased spatial resolution. For comparability, we ran HRLDAS-Crop simulations for all three WRF spatial resolutions. NLDAS climate forcing data was spatially interpolated within HRLDAS-Crop to the three resolutions (25 km, 5 km, 1 km) using bilinear interpolation.

Within Noah-MP, we used the crop model developed by Liu et al. (2016) to simulate the dynamic crop growth of corn and soy over cropland areas as identified by the USGS National Land Cover Dataset (www.mrlc.gov/) provided with WRF 4.0.1. The crop model is run if 50% of a grid cell's area is cultivated, and the grid cell is designated as either corn or soy by the dominant crop type within the cell (Fig. 1). Each year has the same crop distribution because WRF uses static land cover data. Planting and harvest dates are static through time but vary by state. WRF-Crop has eight plant growth stages ranging from pre-planting to post-harvest. Crops progress through each growth stage based on accumulated growing degree day (GDD) thresholds. Plant growth stage GDD thresholds are normalized by an average seasonal GDD map to create a cell-specific GDD threshold that accounts for spatial variations in planted cultivars. The accumulation of leaf, stem, root and grain mass depends on the rate of photosynthesis, experienced environmental stress, and growth stage dependent carbohydrate translocation coefficients (Liu et al., 2016). In this study, we updated the version of Noah-MP with dynamic crop growth provided with WRF 4.0.1 using code from github.com/CharlesZheZhang/hrldas-release. The updated code allows users to assign unique photosynthesis parameters to each crop type, instead of using generic values for all crops, and simulates corn as a C_4 plant. The crop physiology parameters originally provided with WRF-Crop significantly overestimate LAI (Figure S1). We adjusted the provided parameters using estimates derived from literature and decreased the corn coefficient for leaf area per living leaf biomass (BIO2LAI) from 0.035 to 0.02 to best match observed 2015 LAI data from MODIS at the 25 km resolution. We further decreased the soy GDD threshold for plant growth stage progression from seeding to physical maturity (PGS5) from 1555 to 1505 to increase time in grain filling stage. The final crop physiology parameter estimates, with references, are provided in Table S1.

2.2. Model Evaluation

We evaluated WRF-Crop, WRF-DV, and HRLDAS-Crop based on their ability to simulate: (1) the seasonal cycle of temperature, precipitation, LAI, and ET; (2) growing season (May – September) average temperature and total precipitation; (3) July average LAI and ET; (4) county level corn and soy yield. Observed gridded data were upscaled to the corresponding WRF resolution (25 km, 5 km, or 1 km) by first aggregating from their original resolution (Daymet: 1 km or MODIS: 500 m) and then interpolating to the WRF grid using a cubic spline.

Seasonal cycles of temperature and precipitation were calculated as daily domain-averaged temperature and monthly total precipitation for WRF-Crop, WRF-DV, and NLDAS interpolated to the WRF grid. The seasonal cycles of LAI and ET were calculated for either corn or soy grid cells across all three resolutions within the boundaries of D3 (innermost

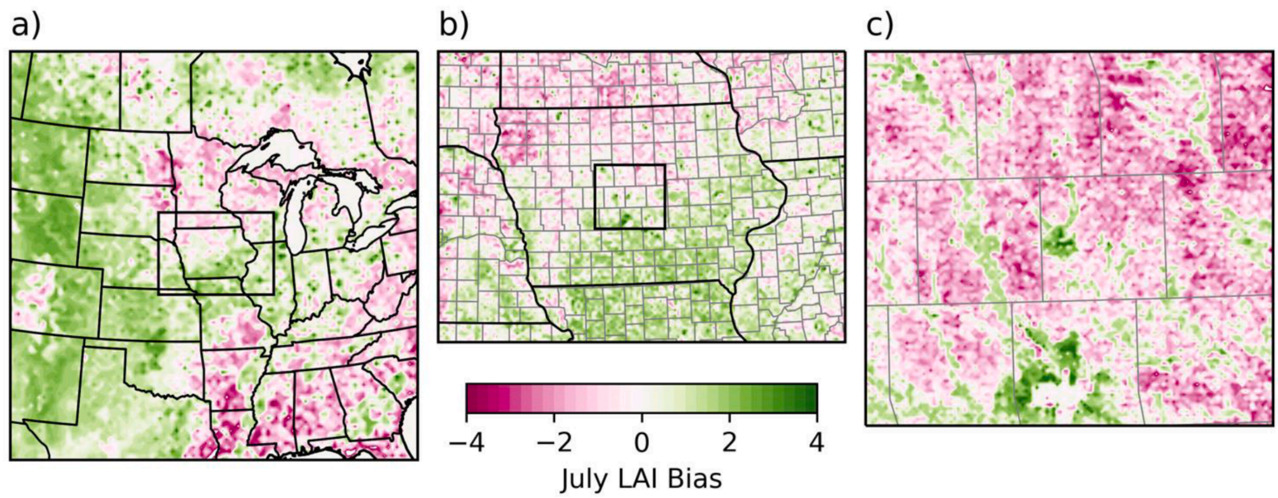

Figure 2. July 2015 LAI bias (simulated – MODIS) for domain 1: 25 km grid (a), domain 2: 5 km grid (b), and domain 3: 1 km grid (c). Bias is relative to MODIS 500m LAI. See Figures S2 and S3 for comparisons in 2010 and 2012. Edge effects were not removed from figures.

domain) to compare consistent geographic areas. WRF uses static crop land use data. To account for the common practice of rotating between corn and soy in a given field, we used data from the Cropland Data Layer (CDL; Boryan, et al., 2011) to mask out any cells that may be misidentified as either corn or soy for a particular year in WRF. Specifically, we calculate the yearly fraction of corn and soy planted within each WRF grid cell using the CDL. We then exclude any WRF grid cells that were modeled with the wrong crop (e.g., simulated as corn but had <50% of its area planted as corn based on CDL data) from comparisons with observations. This classification was performed independently for each of the three nested grid scales, resulting in slightly different distributions of corn and soy for each scale (Fig. 1). To evaluate the model's skill at simulating seasonal cycles, we calculated the Mean Absolute Error (MAE) between the simulated and observed spatially averaged

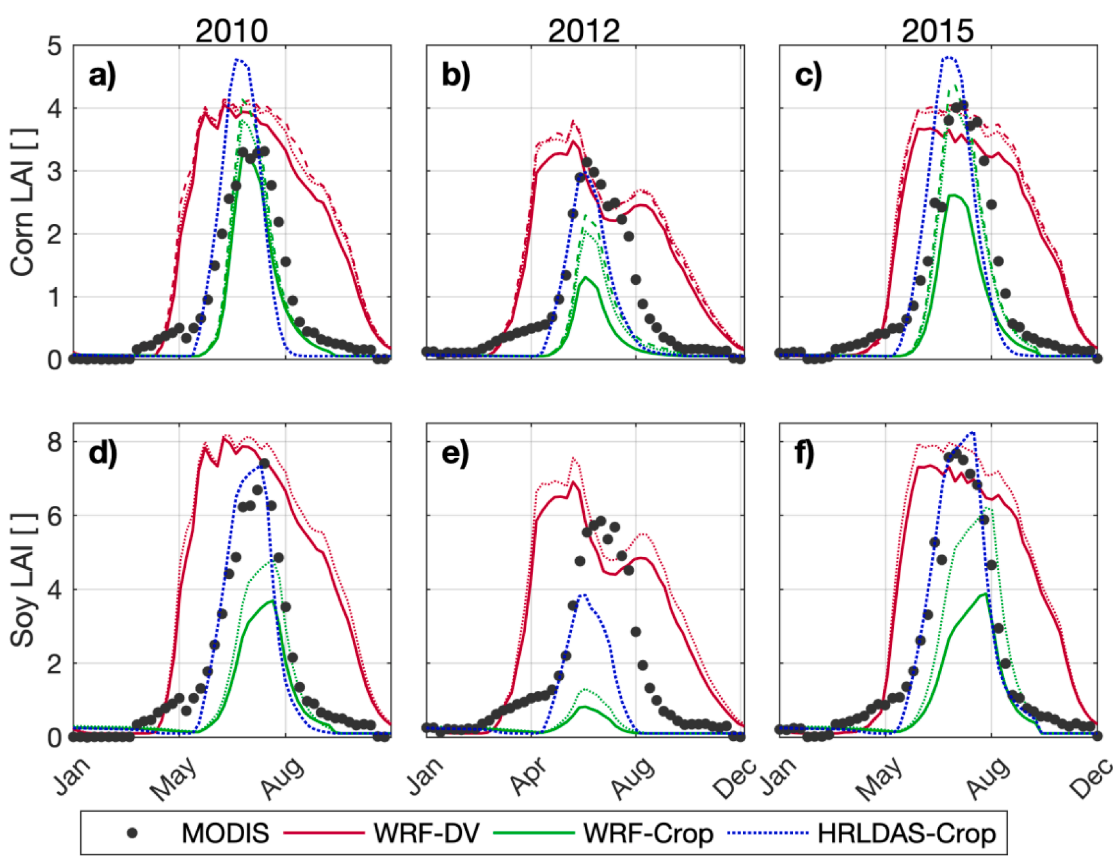

Figure 3. Weekly LAI seasonal cycles for corn (a-c) and soy (d-f). Dashed, dotted, and solid lines correspond with domains 1 (25 km), 2 (5 km), and 3 (1 km) respectively. HRLDAS-Crop is only shown at 5 km resolution. There are no 25 km soy pixels within the boundaries of domain 3, thus there are no dashed lines for panels d-f.

Table 1
Simulated LAI Mean Average Error (MAE) of weekly corn (soy) LAI for each resolution within the boundary of domain 3. No 25 km soy cells exist within the boundaries of domain 3. Simulations with the lowest MAE are shown in bold.

		MAE [ ]		
		2010	2012	2015
WRF- Crop	D1	**0.32** (NA)	0.42(NA)	**0.26** (NA)
	D2	**0.31** (0.77)	0.46 (1.3)	**0.27** (0.81)
	D3	**0.31** (0.97)	0.57 (1.3)	0.50 (1.1)
WRF-DV	D1	1.2 (NA)	0.87 (NA)	0.97 (NA)
	D2	1.1 (2.3)	0.87 (1.8)	0.95 (1.9)
	D3	1.0 (2.0)	0.77 (1.6)	0.86 (1.7)
HRLDAS-Crop	D1	0.33 (NA)	**0.26** (NA)	0.33 (NA)
	D2	0.38 (**0.50**)	**0.29 (0.86)**	0.37 (**0.37**)
	D3	0.38 (**0.50**)	**0.29 (0.89)**	**0.37 (0.37)**

time series.

In addition to the seasonal comparisons, we compared simulated growing season (July) average values of temperature and precipitation (LAI and ET) to upscaled values from Daymet and MODIS. We reported the bias averaged over the entirety of each domain for temperature and precipitation, and the crop-specific bias for ET and LAI. We masked the ten outermost grid cells from WRF simulations to reduce the influence of edge effects.

We compared simulated yield to county-level reported yield from the USDA/NASS website (quickstats.nass.usda.gov). Simulated yield values were aggregated to the county level by spatially averaging any grid cells within a given county that were planted as either corn or soy. Available versions of Noah-MP-Crop do not yet simulate irrigation on the landscape. We do not mask out irrigated counties in our analysis but do separately evaluate simulated yield over irrigated croplands, identified from 2012 USDA NASS census data. Directly comparing simulated yield to reported yield can be problematic, especially over extended time periods, due to the highly trended nature of historical crop yields. However, the direct comparison of yields is desirable due to the ease of interpretation. We reduced the influence of observed yield trends on our comparisons by focusing on three years within a five-year period where yields have remained relatively stable. Average Iowa corn (soy) yields increased insignificantly from 2010 to 2015 by 0.43 (0.048) t/ha/yr (not shown). The interannual variability of yield during this time was high, especially for corn, due to the low reported yields during 2012. Accurately simulating trends in observed yield over longer time periods would require altering crop parameters in WRF-Crop to account for temporal changes in agricultural management or cultivar improvement.

3. Results and Discussion

3.1. Leaf Area Index

LAI, which is defined as the one-sided total leaf area per unit of ground area, affects surface albedo, boundary layer turbulence, and plant transpiration, thus it has a direct connection between the land surface and the atmosphere (Pielke et al., 1998). In Fig. 2, we compare LAI for July 2015 from WRF-Crop across the three simulated spatial resolutions relative to MODIS LAI. Compared to MODIS, WRF-Crop tends to overestimate LAI over the arid western part of D1 and underestimate LAI in the more humid eastern portion. This broad west to east pattern persists for 2010 and 2012 (Figures S2 and S3). July average spatial biases in LAI are summarized in Table S2. Average 2015 July LAI bias over areas planted as corn (soy) is 0.35 (-0.38) for D1, -0.20 (-1.6) for D2 and -1.3 (-4.5) for D3. Both simulated corn and soy appear to be sensitive to drought, as LAI biases are substantially more negative during 2012. July LAI biases over D3 vary spatially and with year simulated. The majority of D3 is planted as corn (Fig. 1), and the LAI bias of corn is variable. However, WRF-Crop consistently underestimates July LAI over soy areas. Soy LAI biases over D3 range from -5.0 in 2012 to -3.6 in 2010 (Tables S2).

We evaluate the seasonal cycles of simulated LAI from WRF-Crop, WRF-DV, and HRLDAS-Crop for corn (panels a-c) and soy (panels d-f) grid cells averaged across the 1 km (D3) domain in Fig. 3. WRF-Crop better captures LAI seasonality and magnitude for corn and soy than WRF-DV. For 2015, D3 corn (soy) MAE is 0.50 (1.1) for WRF-Crop compared to 0.86 (1.7) for WRF-DV (Table 1). However, WRF-Crop underestimates early season corn and soy LAI in all three years. Differences between early season MODIS and WRF-Crop LAI are likely explained by differences in planting dates and crop growth rates. WRF-Crop uses a static planting date of May 7th in Iowa for both corn and soy. Reported USDA NASS data suggest that the majority of the corn acreage (68%) was planted by April 25th in 2010, nearly two weeks earlier than the model date. In 2012, 64% of the corn was planted by May 6th, while in 2015 68% of the corn was planted by May 3rd. WRF-Crop exhibits similar early season LAI biases in 2012 and 2015 despite the model planting date being close to reality. This suggests that early season WRF-Crop LAI biases over corn are associated with a modeled growth rate that is too slow.

For all three years, LAI simulated by WRF-Crop and WRF-DV decreases at higher resolutions for both corn and soy. In most cases, WRF-Crop MAE values are lower for D1 and D2 than for D3. This result is counterintuitive, as the higher resolution of D3 should better capture the

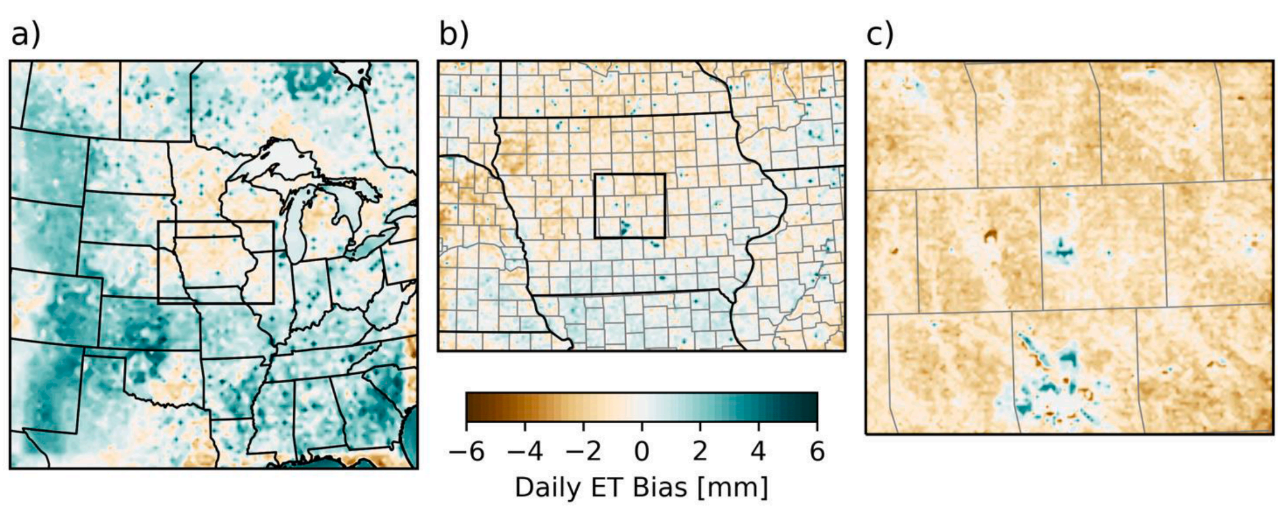

Figure 4. July 2015 ET bias (simulated – MODIS) for domain 1: 25 km grid (a), domain 2: 5 km grid (b), and domain 3: 1 km grid (c) of WRF-Crop. Bias is relative to MODIS 500m ET. See Figures S4 and S5 for comparisons in 2010 and 2012. Edge effects were not removed from figures.

true land use distribution. This contradiction is likely associated with WRF significantly underestimating precipitation at the 1 km scale (Fig. 7). Temperature biases are modest within D3 for 2010 and 2015, but 2012 simulations are substantially warmer than observations (Fig. 6), further limiting simulated LAI during that year. Reduced LAI in D3 translates into a lower MAE for 2010 (Table 1), during which LAI is overestimated in the coarser resolution domains. However, all three spatial resolutions substantially underestimate LAI during the 2012 drought year. Biases in simulated climate account for some of the LAI error. In 2012, corn LAI from HRLDAS-Crop is closer to observations. However, for 2010 and 2015 HRLDAS-Crop overestimates corn and soy LAI.

3.2. Evapotranspiration (ET)

The improved LAI from WRF-crop simulations should translate to a more realistic representation of surface albedo and ET. Liu et al. (2016) show that Noah-MP-Crop has significant improvements in seasonal and diurnal cycles of sensible and latent heat fluxes relative to the dynamic vegetation model. In Fig. 4, we found that there is reasonable agreement between average daily July 2015 ET from MOD16 and WRF-Crop. Simulated average July ET biases in 2015 range from -3.5 mm/day over soy areas in D3 to 1.7 mm/day over soy areas in D1 (Table S3). WRF-Crop overestimates daily July ET over the western and southern portions of D1 and underestimates July ET over croplands in D3. WRF-Crop shows similar spatial patterns in 2010 and 2012 (Figures S4 and S5), however the underestimation of ET over croplands in D3 is more pronounced during the drought year (2012).

In Fig. 5, we compare seasonal ET patterns from MOD16 to simulated values from WRF-Crop, WRF-DV, and HRLDAS-Crop over areas identified as either corn or soy. Monthly averaged ET from the Brooks Field

Table 2
Simulated ET Mean Average Error (MAE) of monthly corn (soy) ET for each resolution within the boundary of domain 3. No 25 km soy cells exist within the boundaries of domain 3. Simulations with the lowest MAE are shown in bold.

		MAE [mm/day]		
		2010	2012	2015
WRF- Crop	D1	**0.74** (NA)	0.86 (NA)	0.83 (NA)
	D2	0.71 **(1.4)**	0.84 (2.1)	0.80 (1.5)
	D3	0.70 (1.4)	0.79 (1.8)	**0.65 (1.3)**
WRF-DV	D1	**0.74** (NA)	0.95 (NA)	**0.78** (NA)
	D2	**0.66 (1.4)**	0.92 (2.0)	**0.77 (1.4)**
	D3	**0.62 (1.3)**	0.83 **(1.7)**	0.75 (1.5)
HRLDAS-Crop	D1	0.97 (NA)	**0.68** (NA)	0.98 (NA)
	D2	0.99 (2.2)	**0.72 (1.7)**	1.0 (2.1)
	D3	0.98 (2.0)	**0.71 (1.7)**	1.0 (2.0)

Site flux tower is strongly correlated with ET from the collocated MOD16 grid cell (Figure S6; 2010 monthly Pearson's correlation = 0.98). Interestingly, the large biases in LAI from the WRF-DV simulations do not translate into an overestimation of overall ET. Instead we find general agreement in simulated ET between WRF-Crop and WRF-DV simulations, both of which are strongly correlated with MODIS data. WRF-Crop MAE slightly improves with resolution and is generally comparable to WRF-DV (Table 2). Partitioning ET into distinct moisture sources (i.e., canopy evaporation, bare ground evaporation, and transpiration) does reveal differences between WRF-Crop and WRF-DV (Figures S7 – S9). Consistent with the differences in LAI, WRF-DV tends to simulate higher rates of transpiration early and late in the growing season as vegetation is not bound by planting and harvest dates.

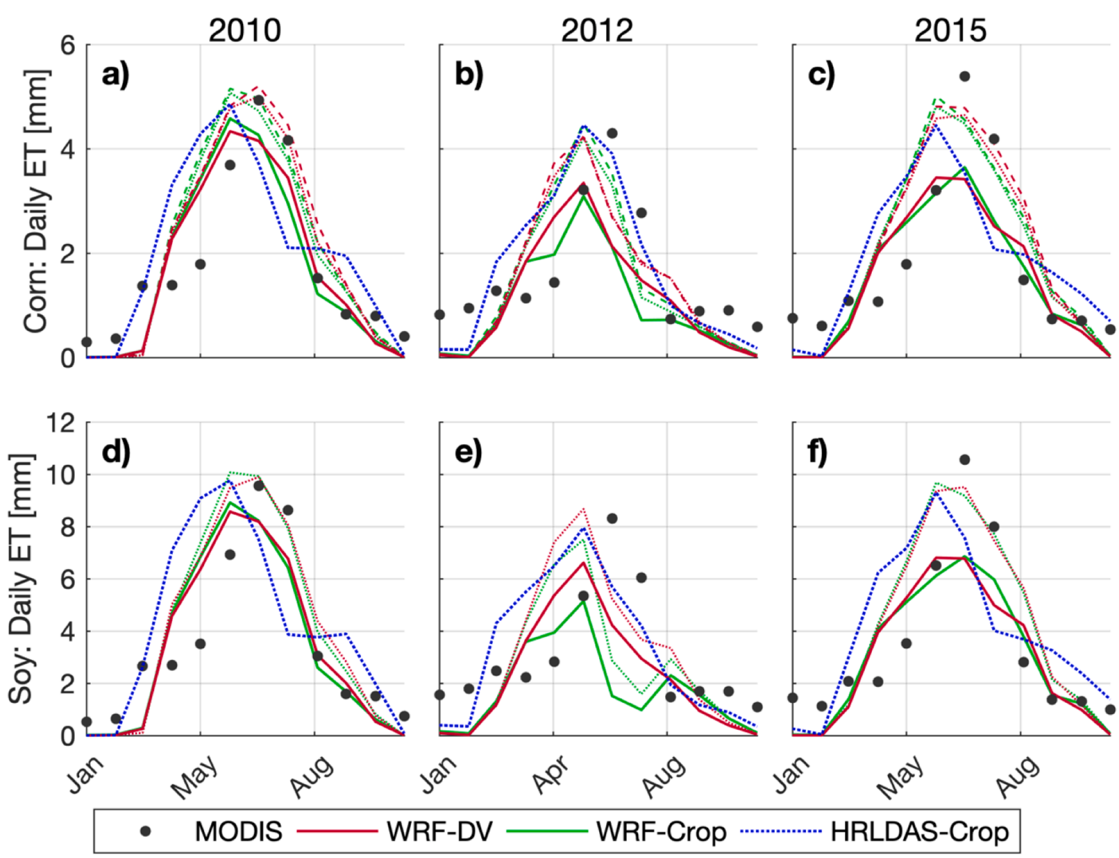

Figure 5. Monthly seasonal cycles of average daily ET for corn (a-c) and soy (d-f). Dashed, dotted, and solid lines correspond with domains 1 (25 km), 2 (5 km), and 3 (1 km) respectively. HRLDAS-Crop only shown at 5 km resolution. There are no 25 km soy pixels within the boundaries of domain 3, thus there are no dashed lines for panels d-f.

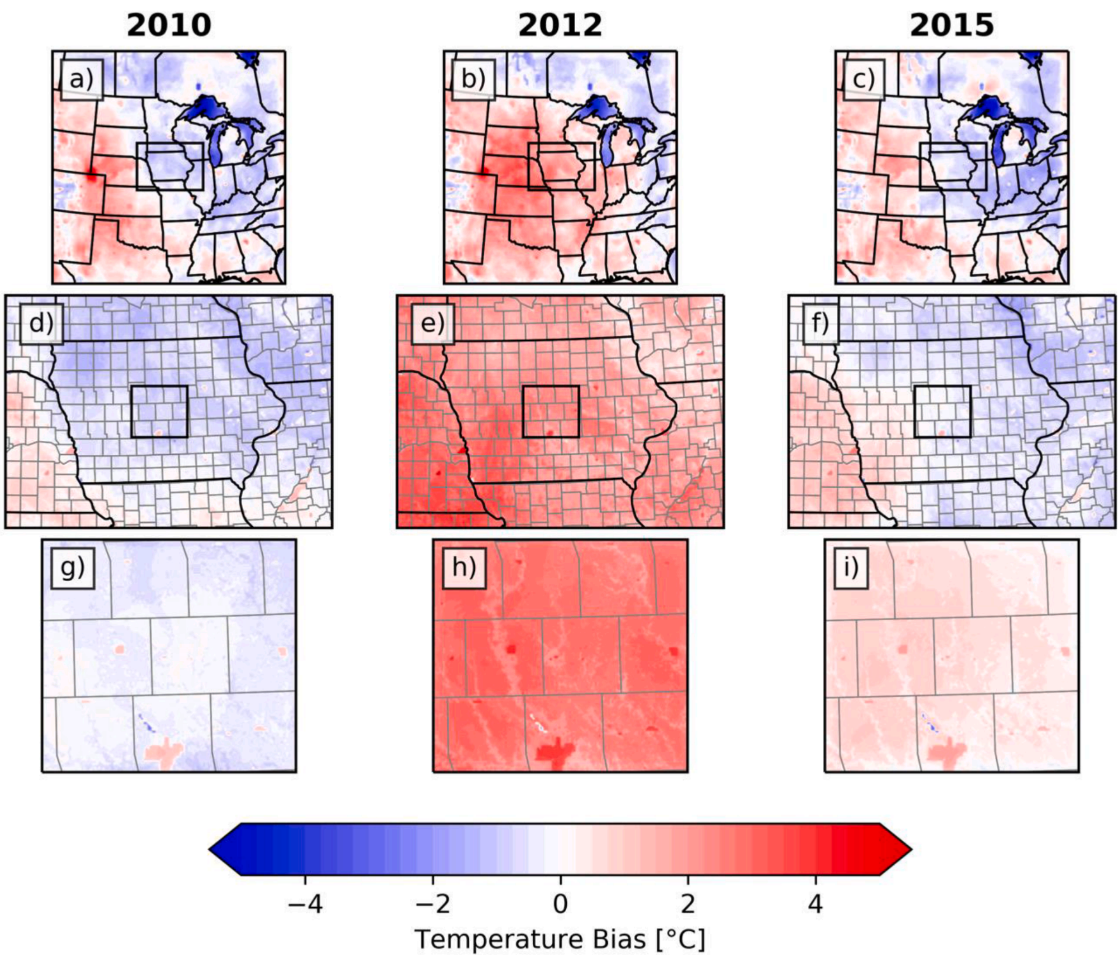

Figure 6. WRF-Crop May through September average temperature bias (simulated - Daymet) for each year simulated. Domain 1 (25 km) with domain 2 identified as a black box (a-c), domain 2 (5 km) with counties outlined in grey and domain 3 identified as black box (d-f), and domain 3 (1 km) with county borders outlined in grey (g-i). Edge effects were not removed from figures.

3.3. Temperature and Precipitation

Fig. 6 shows WRF-Crop average temperature biases relative to Daymet for May through September, which is the approximate growing season over the majority of our domain. WRF-DV growing season temperature biases are shown in Figure S10. For 2015, WRF-Crop overestimates growing season temperatures across most of the Great Plains by roughly 1-2°C and slightly underestimates temperature in the Midwest. The 2015 average simulated temperature is 0.21°C cooler than Daymet over D2 and 0.56°C warmer over the 15 counties included in D3 (Table S4). WRF-Crop substantially overestimates temperatures for 2012, an anomalously warm and dry year for the central U.S., over the majority of D1 and practically all of D2 and D3. The 2012 growing season temperature biases are 0.59°C, 2.0°C, and 2.7°C for D1, D2, and D3, respectively (Table S4). Note that the city of Des Moines Iowa, near the southern border of D3 is anomalously warm in 2010, 2012, and 2015. These grid points are assigned an albedo typical of urban areas, however we do not use an urban parameterization scheme for these simulations, which could explain the localized warm bias. While there is little difference in daily temperatures between WRF-Crop and WRF-DV (Figures S11 – S13), WRF-Crop has a slightly lower MAE in simulated daily average temperature (Table 3). Note that because HRLDAS-Crop does not simulate temperature, forcing data for those simulations derived from NLDAS are shown for comparison.

Table 3
Mean Absolute Error (MAE) in domain averaged timeseries of simulated daily temperature and total monthly precipitation. The ten outermost grid cells on each side were removed from WRF simulations to reduce edge effects. Simulations with the lowest MAE are shown in bold.

		May – September**MAE**					
		Temperature [°C]			Precipitation [mm]		
		2010	2012	2015	2010	2012	2015
WRF- Crop	D1	**0.54**	**0.81**	**0.59**	26	6.8	15
	D2	**1.1**	3.1	0.94	30	17	19
	D3	**1.4**	3.8	**1.3**	100	27	64
WRF-DV	D1	0.79	0.82	0.57	25	6.6	16
	D2	1.2	**3.0**	**0.94**	30	16	19
	D3	1.6	**3.6**	1.4	106	24	69
NLDAS*	D1	1.4	1.8	1.4	**7.6**	**5.4**	**9.6**
	D2	1.7	3.6	1.8	**7.3**	**7.2**	**9.5**
	D3	1.7	4.2	1.8	**18**	**6.9**	**14**

* NLDAS values have been interpolated to WRF grid.

Fig. 7 shows total growing season precipitation (May – September) simulated by WRF-Crop relative to Daymet for each domain. Precipitation spatial biases over D1 are generally heterogeneous with the exception of clear edge effects and a consistent wet bias in the southeastern corner for all years. Domain average biases for D1 are 19.0 mm for 2010, 10.4 mm for 2012, and 15.0 mm for 2015 (Table S4). Total growing season precipitation bias over D2 is also heterogeneous. Domain 2 biases are 0.876 mm for 2010, 7.22 mm for 2012 and 13.6 mm for 2015. Domain 3 shows a significant and consistent dry bias for all three years. Domain 3 biases are -37.1 mm for 2010, -41.4 mm for 2012, and -37.3 mm for 2015. Note that the edge effects apparent in all figures

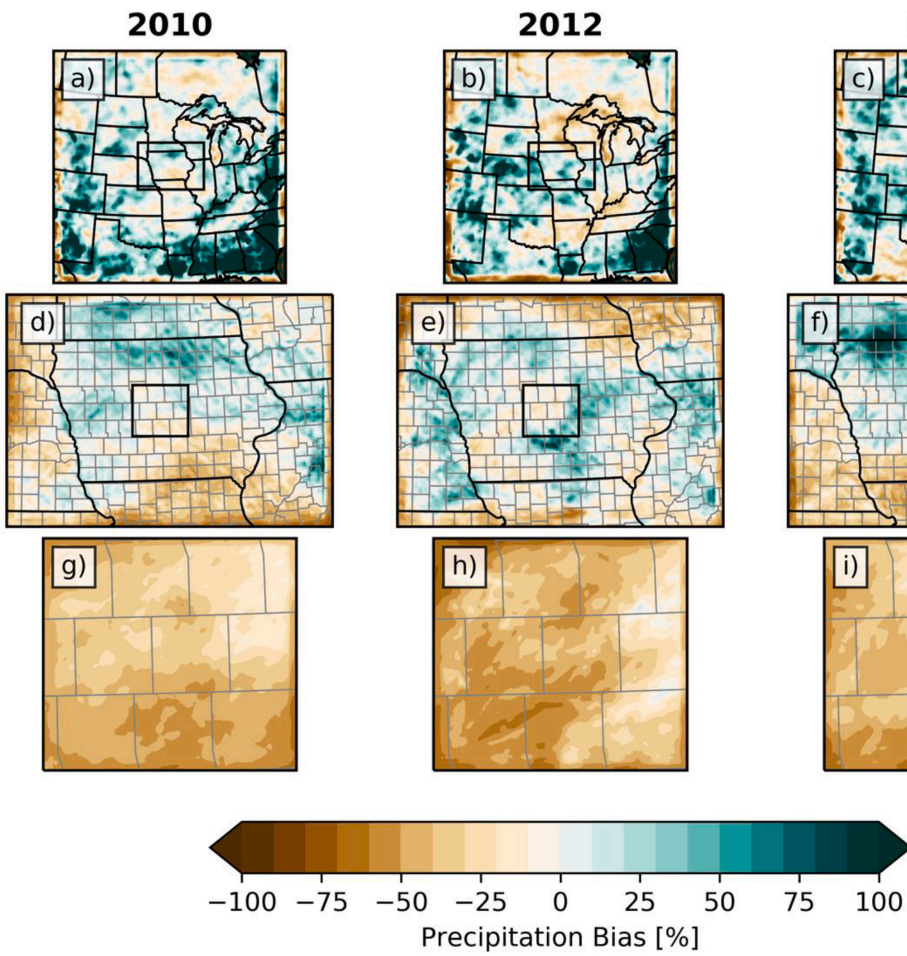

Figure 7. May through September total precipitation bias (simulated - Daymet) for each year simulated. Domain 1 (25 km) with domain 2 identified as black box (a-c), domain 2 (5 km) with Iowa counties outlined in grey and domain 3 identified as black box (d-f), and domain 3 (1 km) with county borders outlined in grey (g-i). Edge effects were not removed from figures.

were removed before calculating bias and MAE. Table 3 highlights to MAE from total monthly precipitation timeseries for 2010, 2012, and 2015 shown in Figures S14-S16. Both WRF-Crop and WRF-DV have a substantially higher MAE than NLDAS, especially over D3, relative to Daymet, but there is little difference in total monthly precipitation between WRF-Crop and WRF-DV.

3.4. Yield

In addition to more realistically capturing land-atmosphere interactions over croplands, WRF-Crop is able to directly simulate grain yield for corn and soy. Reliably using climate models such as WRF for future yield projections requires an understanding of biases. We compare simulated yield from WRF-Crop and HRLDAS-Crop to reported yield for 2015 in Fig. 8 and summarize yield bias results from all simulations in Table 4. Yield bias maps for 2010 and 2012 are shown in Figures S17 and S18, respectively, and correlation plots for all simulations are shown in Figures S19 and S20 with yield MAE and line of best fit statistics in Table S5. In 2015, WRF-Crop has an average simulated corn (soy) bias of -3.1 (0.79) t/ha over D1, -4.2 (-0.25) t/ha over D2, and -6.2 (-1.3) t/ha over D3. WRF-Crop corn (soy) yield MAE in 2015 is nearly identical in magnitude to yield bias, 3.2 (1.1) t/ha over D1, 4.2 (0.90) t/ha over D2, and 6.2 (1.3) t/ha over D3, underscoring the consistent underestimation of yield, especially for corn (Table S5). However, simulated yield biases from WRF-Crop are compounded by errors in simulated climate. HRLDAS-Crop simulations reduce these biases to -2.0 (0.035) t/ha for D1, -1.9 (0.22) t/ha for D2, and -0.87 (0.49) t/ha for D3. Corn yields are routinely underestimated throughout nearly all counties in WRF-Crop and HRLDAS-Crop, with the exception of southeastern Iowa and western Illinois in 2010 (Fig S17). However, there is considerable spatial heterogeneity in soy yield error. HRLDAS-Crop tends to underestimate soy yields in D1, however D2 counties in southern Iowa and all counties in D3 are slightly overestimated in 2015 and 2010. Simulated crop yields are highly sensitive to drought. In 2012, corn and soy are underestimated for nearly all counties in both HRLDAS-Crop and WRF-Crop. This underestimation is nearly twice as large in WRF-Crop relative to HLRDAS-Crop, exacerbated by hot and dry biases in WRF (Table 4 and Figs. 6 and 7). Simulated irrigation within Noah-MP was not available at the time of this study. Not surprisingly, the most significant yield biases for WRF-Crop and HRLDAS-Crop occur in irrigated counties, defined here as counties with an irrigated fraction greater than 25%. Yield biases are significantly more negative ($p< 0.01$) in these irrigated counties than the remaining, non-irrigated counties, for WRF-Crop and HRLDAS-Crop over D1 and D2 (Table 4 and Figure S21). There are no counties with an irrigated fraction greater than 25% in D3.

Overall, our results are consistent with those of Zhang et al. (2020), who found that the offline version of Noah-MP-Crop without irrigation forced with meteorological data from NLDAS produced average 2000-2004 yield errors of 26.3% for corn and 27.1% for soy based on RSME values. Here we compare individual growing seasons and find domain average yield MAE from HRLDAS-Crop ranges from 0.91 t/ha (2015 D3) to 3.9 t/ha (2012 D3) for corn and 0.40 t/ha (2010 D1) to 1.0 t/ha (2010 D3) for soy (Table S5). As a percentage of the mean annual

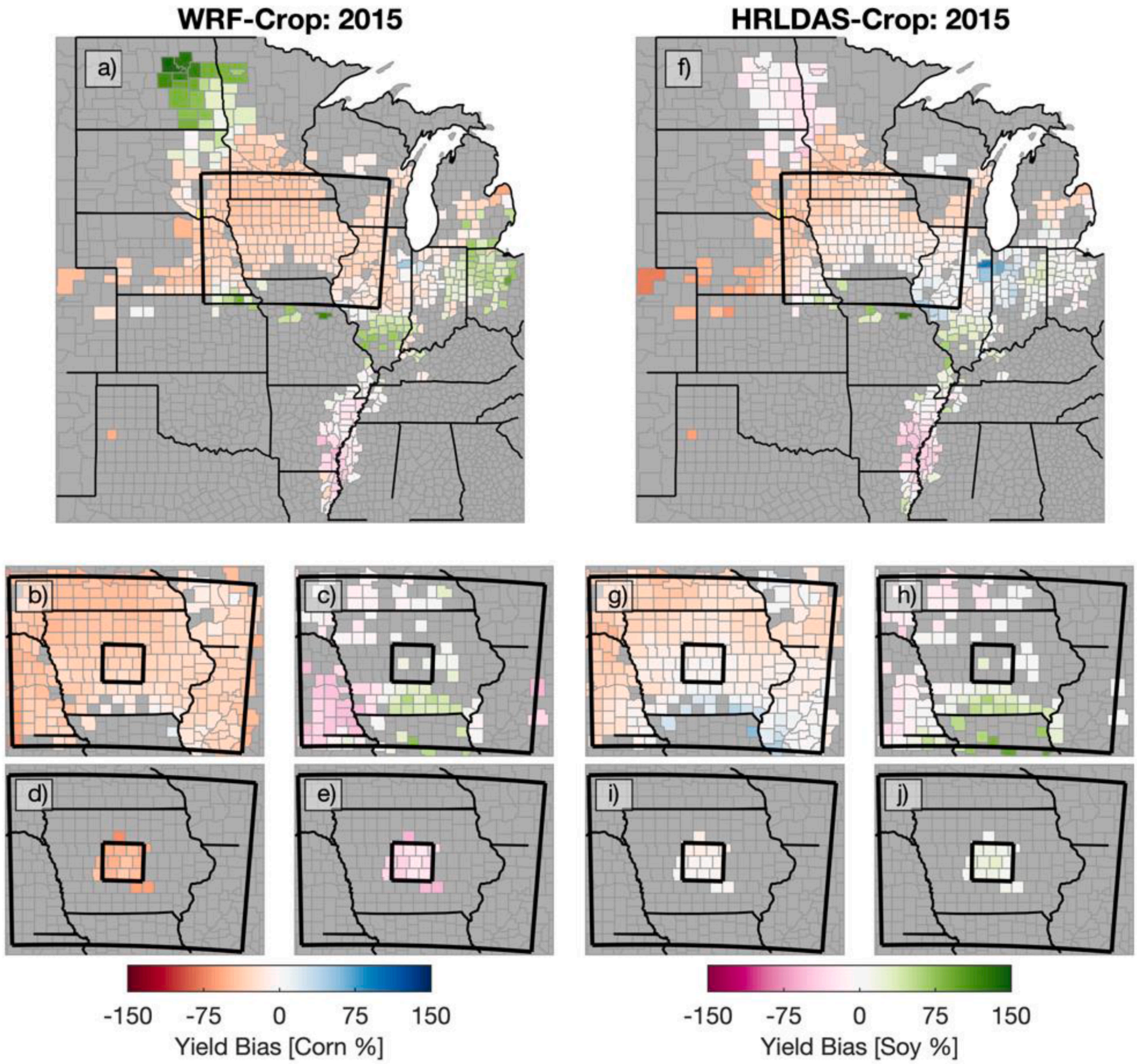

Figure 8. Simulated yield bias for 2015 shown as a percentage of observed county yield from: WRF-Crop (a-e) and HRLDAS-Crop (f-j). County yield biases in domain 1 (25 km grid; panels a and f) contain both corn and soy grid cells. County yield biases in domain 2 (5 km grid; panels b,c,g,h) for corn (panels b and g) and soy (panels c and h) grid cells. County yield bias in domain 3 (1 km grid; panels d,e,i,j) for corn (panels d and i) and soy (panels e and j) grid cells. Observed yield from USDA-NASS. Black boxes identify domain boundaries. We include all counties that contain any WRF grid cells simulating crops.

Table 4
Simulated yield average bias for corn (soy) from WRF-Crop and HRLDAS-Crop over both all counties within a domain and irrigated counties (Irrigated fraction >= 25%) within a domain. Average yearly yield is included for reference. WRF-DV does is excluded from this table as it does not simulate crop yield. Simulations withe the lowest absolute bias are shown in bold.

		2010 Bias [t/ha]		2012 Bias [t/ha]		2015 Bias [t/ha]	
		All	Irrigated	All	Irrigated	All	Irrigated
WRF-Crop	D1	-1.9 (0.31)	-3.1 (-0.76)	-4.7 (-1.9)	-7.5 (-2.2)	-3.1 (0.79)	-3.9 (-0.53)
	D2	-2.4 (-0.29)	-3.9 (-1.3)	-5.1 (-2.1)	-6.7 (-2.4)	-4.2 (-0.25)	-5.3 (-1.7)
	D3	-3.0 **(-0.10)**	NA (NA)	-7.2 (-2.9)	NA (NA)	-6.2 (-1.3)	NA (NA)
HRLDAS-Crop	D1	**-0.35 (-0.12)**	-3.1 (-0.47)	**-2.6 (-0.56)**	-5.7 (-1.3)	**-2.0 (0.035)**	-4.1 (-0.66)
	D2	**0.63 (0.25)**	-2.1 (-0.90)	**-2.8 (-0.58)**	-4.7 (-0.93)	**-1.9 (0.22)**	-3.2 (-0.74)
	D3	**2.4** (1.0)	NA (NA)	**-3.9 (-0.99)**	NA (NA)	**-0.87 (0.49)**	NA (NA)
USDA Average		8.15 (2.67)		7.08 (2.64)		9.48 (3.02)	

yield, these ranges translate to 9.6% – 55.1% for corn and 15.0% – 37.5% for soy. Domain average yield MAE from WRF-Crop ranges from 2.1 t/ha (2010 D1) to 7.2 t/ha (2012 D3) for corn and 0.75 t/ha (2010 D2) to 2.9 t/ha (2012 D3) for soy, or 25.7% – 102% for corn and 28.1% – 109% for soy.

We evaluated the effect of model resolution on yield estimates by comparing simulated yield in the 15 counties within the domain boundary of D3, across the three spatial resolutions (25 km, 5 km, 1 km;

Figures S19 and S20). In WRF-Crop, finer resolution routinely results in reduced corn and soy yield. This translates into a larger negative yield bias for corn, which is consistently underestimated in WRF-Crop. Coarser resolution simulations aggregate temperature and precipitation across a broader area, suppressing localized extremes and producing a drizzling effect of precipitation, both of which likely enhance plant growth (Challinor, et al., 2009). HRLDAS-Crop shows little difference in simulated yield across resolutions as the meteorological forcing data are simply interpolated, not dynamically downscaled as in WRF.

4. Conclusion

Agricultural practices alter the hydrologic and carbon cycles with notable feedbacks on climate. Over the last decade, Earth system models have begun to explicitly represent crop growth, allowing for more realistic representations of land-atmosphere interactions over agricultural areas and crop yield simulations. Here, we evaluate the ability of dynamic crop growth in Noah-MP, both coupled and decoupled from WRF. Dynamic crop growth in WRF substantially improves simulated LAI of both corn and soy over the central U.S. The differences in LAI seasonality and extent lead to differences in evapotranspiration partitioning between WRF-DV and WRF-Crop. However, these differences are largely balanced as there is no distinct difference in total ET between WRF with dynamic vegetation and WRF with dynamic crop growth for these model domains. Simulated ET from WRF-Crop and WRF-DV have similar MAE over corn and soy areas when compared to MODIS. Consequently, there is little difference in simulated temperature and precipitation between WRF simulations with and without dynamic crop growth.

Compared to reported county level yields, WRF-Crop underestimates corn yields at all three resolutions. Modeled soy yields are closer to reported yields. Finer resolutions within WRF-Crop led to lower, and therefore generally worse, yield estimates for both corn and soy. WRF-Crop is sensitive to drought stress as simulated yield and LAI for both corn and soy are substantially below observations for 2012. Yield estimates within WRF-Crop are a function of the representation of crop physiology, agricultural management, and biases in simulated climate, making it difficult to directly compare to observations. Biases in simulated climate substantially contributed to simulated yield error. Running Noah-MP-Crop forced with reanalysis removes biases in simulated climate and reduces corn and soy yield error. The addition of dynamic crop growth to Noah-MP is a significant improvement in representing the land surface in WRF. Future work could refine agricultural management practices by integrating irrigation, allowing for dynamic planting and harvest dates, and incorporating variable fertilizations rates.

Data Availability Statement

WRF 4.0.1 code can be downloaded from (github.com/wrf-model/WRF/releases) and HRLDAS code can be downloaded from (github.com/NCAR/hrldas-release). ERA-I data are available at (www.ecmwf.int/). NLDAS data are available at (ldas.gsfc.nasa.gov/nldas). Daymet data are available at (daymet.ornl.gov/). The Cropland Data Layer can be downloaded from (www.nass.usda.gov/Research_and_Science/Cropland/SARS1a.php). The AmeriFlux site data (US-Br1) are available from the AmeriFlux website (ameriflux. lbl.gov/). The county-level crop yield, irrigated area, and cropland area data are available from USDA/NASS website (quickstats.nass.usda.gov/). MODIS LAI and ET data were acquired through the USGS and NASA Application for Extracting and Exploring Analysis Ready Samples (lpdaac.usgs.gov/tools/appeears/).

Declaration of Competing Interest

The authors declare that they have no known competing financial interests or personal relationships that could have appeared to influence the work reported in this paper.

Acknowledgements

This study was funded by the United States Department of Agriculture National Institute of Food and Agriculture (2015-68007-23133 and 2018-67003-27406), National Science Foundation (BCS 184018), and Nelson A. Rockefeller Center at Dartmouth College. This paper benefits from data and code provided by the National Center for Atmospheric Research, European Centre for Medium-Range Weather Forecasts, National Aeronautics and Space Administration, United States Department of Agriculture, United States Department of Energy, and United States Geological Survey. We thank Prof. Stephanie Spera (University of Richmond) and Research Computing staff at Dartmouth College for their assistance with compiling and running WRF.

Supplementary materials

Supplementary material associated with this article can be found, in the online version, at doi:10.1016/j.agrformet.2020.108217.

References

Adegoke, J.O., Pielke, R., Carleton, A.M., 2007. Observational and modeling studies of the impacts of agriculture-related land use change on planetary boundary layer processes in the central U.S. Agricultural and Forest Meteorology 142 (2–4), 203–215. https://doi.org/10.1016/j.agrformet.2006.07.013.

Alter, R.E., Douglas, H.C., Winter, J.M., Eltahir, E.A.B., 2018. Twentieth Century Regional Climate Change During the Summer in the Central United States Attributed to Agricultural Intensification. Geophysical Research Letters 45 (3), 1586–1594. https://doi.org/10.1002/2017GL075604.

Berrisford, P., Dee, D. P., Poli, P., Brugge, R., Fielding, M., Fuentes, M., … Simmons, A. (2011). The ERA-Interim archive Version 2.0, (1), 23. Retrieved from https://www.ecmwf.int/node/8174.

Bonan, G.B., 2008. Forests and climate change: Forcings, feedbacks, and the climate benefits of forests. Science. https://doi.org/10.1126/science.1155121.

Boryan, C., Yang, Z., Mueller, R., Craig, M., 2011. Monitoring US agriculture: the US Department of Agriculture, National Agricultural Statistics Service, Cropland Data Layer Program. Geocarto International 26 (5), 341–358. https://doi.org/10.1080/10106049.2011.562309.

Boucher, O., Myhre, G., Myhre, A., 2004. Direct human influence of irrigation on atmospheric water vapour and climate. Climate Dynamics 22 (6–7), 597–603. https://doi.org/10.1007/s00382-004-0402-4.

Bukovsky, M.S., Karoly, D.J., 2011. A Regional Modeling Study of Climate Change Impacts on Warm-Season Precipitation in the Central United States. Journal of Climate 24 (7), 1985–2002. https://doi.org/10.1175/2010JCLI3447.1.

Challinor, A.J., Ewert, F., Arnold, S., Simelton, E., Fraser, E., 2009. Crops and climate change: Progress, trends, and challenges in simulating impacts and informing adaptation. Journal of Experimental Botany 60, 2775–2789. Oxford Academic. https://doi.org/10.1093/jxb/erp062.

Chen, F., Manning, K.W., LeMone, M.A., Trier, S.B., Alfieri, J.G., Roberts, R., Blanken, P. D., 2007. Description and Evaluation of the Characteristics of the NCAR High-Resolution Land Data Assimilation System. Journal of Applied Meteorology and Climatology 46 (6), 694–713. https://doi.org/10.1175/JAM2463.1.

Chen, X., Jeong, S.J., 2018. Irrigation enhances local warming with greater nocturnal warming effects than daytime cooling effects. Environmental Research Letters 13 (2). https://doi.org/10.1088/1748-9326/aa9dea.

Dieter, C. A., Maupin, M. A., Caldwell, R. R., Harris, M. A., Ivahnenko, T. I., Lovelace, J. K., … Linsey, K. S. (2018). *Estimated use of water in the United States in 2015. Circular*. Reston, VA. https://doi.org/10.3133/cir1441.

Drewniak, B., Song, J., Prell, J., Kotamarthi, V.R., Jacob, R., 2013. Modeling agriculture in the Community Land Model. Geoscientific Model Development 6 (2), 495–515. https://doi.org/10.5194/gmd-6-495-2013.

FAO. (2017). *Water for Sustainable Food and Agriculture A report produced for the G20 Presidency of Germany*. Retrieved from www.fao.org/publications.

Foley, J.A., DeFries, R., Asner, G.P., Barford, C., Bonan, G., Carpenter, S.R., Stuart Chapin, F., Coe, M.T., Daily, G.C., Gibbs, H.K., Helkowski, J.H., Holloway, T., Howard, E.A., Kucharik, C.J., Monfreda, C., Patz, J.A., Colin Prentice, I., Ramankutty, N., Snyder, P.K., 2005. Global consequences of land use. Science (309), 570–574. https://doi.org/10.1126/science.1111772.

Harding, K.J., Twine, T.E., Lu, Y., 2015. Effects of Dynamic Crop Growth on the Simulated Precipitation Response to Irrigation. Earth Interactions 19 (14), 1–31. https://doi.org/10.1175/EI-D-15-0030.1.

Huang, H., Winter, J.M., Osterberg, E.C., Hanrahan, J., Bruyère, C.L., Clemins, P., Beckage, B., 2020. Simulating precipitation and temperature in the Lake Champlain basin using a regional climate model: limitations and uncertainties. Climate Dynamics 54 (1–2), 69–84. https://doi.org/10.1007/s00382-019-04987-8.

Hutchinson, T.A., 2007. An Adaptive Time-Step for Increased Model Efficiency. Extended Abstracts, Eighth WRF Users' Workshop 4.

Kucharik, C., 2003. Evaluation of a process-based agro-ecosystem model (Agro-IBIS) across the US corn belt: simulations of the interannual variability in maize yield. Earth Interact 7, 1–33. https://doi.org/10.1175/1087-3562(2003)007<0001:eoapam>2.0.co.

Kueppers, L.M., Snyder, M.A., Sloan, L.C., 2007. Irrigation cooling effect: Regional climate forcing by land-use change. Geophysical Research Letters 34 (3). https://doi.org/10.1029/2006GL028679.

Levis, S., Gordon, B.B., Kluzek, Erik, Thornton, P.E., Jones, A., Sacks, W.J., Kucharik, C. J., 2012. Interactive Crop Management in the Community Earth System Model (CESM1): Seasonal influences on land-atmosphere fluxes. Journal of Climate 25 (14), 4839–4859. https://doi.org/10.1175/JCLI-D-11-00446.1.

Liu, X., Chen, F., Barlage, M., Zhou, G., Niyogi, D., 2016. Noah-MP-Crop: Introducing dynamic crop growth in the Noah-MP land surface model. Journal of Geophysical Research: Atmospheres 121 (23), 13953–13972. https://doi.org/10.1002/2016JD025597.

Lobell, D.B., Schlenker, W., Costa-Roberts, J., 2011. Climate trends and global crop production since 1980. Science 333 (6042), 616–620. https://doi.org/10.1126/science.1204531.

Lu, Y., Jin, J., Kueppers, L.M., 2015. Crop growth and irrigation interact to influence surface fluxes in a regional climate-cropland model (WRF3.3-CLM4crop). Climate Dynamics 45 (11–12), 3347–3363. https://doi.org/10.1007/s00382-015-2543-z.

Luo, L., Robock, A., Mitchell, K.E., Houser, P.R., Wood, E.F., Schaake, J.C., Tarpley, J.D., 2003. Validation of the North American Land Data Assimilation System (NLDAS) retrospective forcing over the southern Great Plains. Journal of Geophysical Research D: Atmospheres 108 (22). https://doi.org/10.1029/2002jd003246.

McDermid, S.S., Mearns, L.O., Ruane, A.C., 2017. Representing agriculture in Earth System Models: Approaches and priorities for development. Journal of Advances in Modeling Earth Systems. Blackwell Publishing Ltd. https://doi.org/10.1002/2016MS000749.

Mu, Q., Heinsch, F.A., Zhao, M., Running, S.W., 2007. Development of a global evapotranspiration algorithm based on MODIS and global meteorology data. Remote Sensing of Environment 111 (4), 519–536. https://doi.org/10.1016/j.rse.2007.04.015.

Mu, Q., Zhao, M., Running, S.W., 2011. Improvements to a MODIS global terrestrial evapotranspiration algorithm. Remote Sensing of Environment 115 (8), 1781–1800. https://doi.org/10.1016/j.rse.2011.02.019.

Mueller, N.D., Butler, E.E., McKinnon, K.A., Rhines, A., Tingley, M., Holbrook, N.M., Huybers, P., 2016. Cooling of US Midwest summer temperature extremes from cropland intensification. Nature Climate Change 6 (3), 317–322. https://doi.org/10.1038/nclimate2825.

Myneni, R., Knyazikhin, Y., Park, T. (2015). MOD15A2H MODIS/Terra Leaf Area Index/FPAR 8-Day L4 Global 500m SIN Grid V006. NASA EOSDIS Land Processes DAAC. Accessed 2020-05-08 from https://doi.org/10.5067/MODIS/MOD15A2H.006.

Nikiel, C.A., Eltahir, E.A.B., 2019. Summer Climate Change in the Midwest and Great Plains due to Agricultural Development during the Twentieth Century. Journal of Climate 32 (17), 5583–5599. https://doi.org/10.1175/JCLI-D-19-0096.1.

Niu, G.Y., Yang, Z.L., Mitchell, K.E., Chen, F., Ek, M.B., Barlage, M., Xia, Y., 2011. The community Noah land surface model with multiparameterization options (Noah-MP): 1. Model description and evaluation with local-scale measurements. Journal of Geophysical Research Atmospheres 116 (12). https://doi.org/10.1029/2010JD015139.

Osborne, T., Slingo, J., Lawrence, D., Wheeler, T., 2009. Examining the interaction of growing crops with local climate using a coupled crop-climate model. Journal of Climate 22 (6), 1393–1411. https://doi.org/10.1175/2008JCLI2494.1.

Otterman, J., 1977. Anthropogenic impact on the albedo of the earth. Climatic Change 1 (2), 137–155. https://doi.org/10.1007/BF01884408.

Partridge, T.F., Winter, J.M., Osterberg, E.C., Hyndman, D.W., Kendall, A.D., Magilligan, F.J., 2018. Spatially Distinct Seasonal Patterns and Forcings of the U.S. Warming Hole. Geophysical Research Letters 45 (4), 2055–2063. https://doi.org/10.1002/2017GL076463.

Partridge, Trevor F., Winter, J.M., Liu, L., Kendall, A.D., Basso, B., Hyndman, D.W., 2019. Mid-20th century warming hole boosts US maize yields. Environmental Research Letters. https://doi.org/10.1088/1748-9326/ab422b.

Pei, L., Moore, N., Zhong, S., Kendall, A.D., Gao, Z., Hyndman, D.W., 2016. Effects of Irrigation on Summer Precipitation over the United States. Journal of Climate 29 (10), 3541–3558. https://doi.org/10.1175/JCLI-D-15-0337.1.

Pielke, R.A., Sr, ., Avissar, R., Raupach, M., Dolman, A.J., Zeng, X., Denning, A.S., 1998. Interactions between the atmosphere and terrestrial ecosystems: influence on weather and climate. Global Change Biology 4 (5), 461–475. https://doi.org/10.1046/j.1365-2486.1998.t01-1-00176.x.

Pieri, A.B., von Hardenberg, J., Parodi, A., Provenzale, A., 2015. Sensitivity of Precipitation Statistics to Resolution, Microphysics, and Convective Parameterization: A Case Study with the High-Resolution WRF Climate Model over Europe. Journal of Hydrometeorology 16 (4), 1857–1872. https://doi.org/10.1175/JHM-D-14-0221.1.

Puma, M., Cook, B.I., 2010. Effects of irrigation on global climate during the 20th century. Article in Journal of Geophysical Research Atmospheres 115, 16120. https://doi.org/10.1029/2010JD014122.

Ramoelo, A., Majozi, N., Mathieu, R., Jovanovic, N., Nickless, A., Dzikiti, S., 2014. Validation of Global Evapotranspiration Product (MOD16) using Flux Tower Data in the African Savanna, South Africa. Remote Sensing 6 (8), 7406–7423. https://doi.org/10.3390/rs6087406.

Rosenzweig, C., Parry, M.L., 1994. Potential impact of climate change on world food supply. Nature 367 (6459), 133–138. https://doi.org/10.1038/367133a0.

Running, S., Mu, Q., Zhao, M. (2017). MOD16A2 MODIS/Terra Net Evapotranspiration 8-Day L4 Global 500m SIN Grid V006. NASA EOSDIS Land Processes DAAC. Accessed 2020-05-08 from https://doi.org/10.5067/MODIS/MOD16A2.006.

Siebert, S., Burke, J., Faures, J.M., Frenken, K., Hoogeveen, J., Döll, P., Portmann, F.T., 2010. Groundwater use for irrigation - A global inventory. Hydrology and Earth System Sciences 14 (10), 1863–1880. https://doi.org/10.5194/hess-14-1863-2010.

Skamarock, W. C., Klemp, J. B., Dudhia, J., Gill, D. O., Barker, D. M., Duda, M. G., … Powers, J. G. (2019). A Description of the Advanced Research WRF Version 4. https://doi.org/10.6084/M9.FIGSHARE.7369994.V4.

Spera, S.A., Winter, J.M., Partridge, T.F., 2020. Brazilian maize yields negatively affected by climate after land clearing. Nature Sustainability 1–8. https://doi.org/10.1038/s41893-020-0560-3.

Sun, Z., Wang, Q., Ouyang, Z., Watanabe, M., Matsushita, B., Fukushima, T., 2007. Evaluation of MOD16 algorithm using MODIS and ground observational data in winter wheat field in North China Plain. Hydrological Processes 21 (9), 1196–1206. https://doi.org/10.1002/hyp.6679.

Thiery, W., Davin, E.L., Lawrence, D.M., Hirsch, A.L., Hauser, M., Seneviratne, S.I., 2017. Present-day irrigation mitigates heat extremes. Journal of Geophysical Research 122 (3), 1403–1422. https://doi.org/10.1002/2016JD025740.

Thiery, W., Visser, A.J., Fischer, E.M., Hauser, M., Hirsch, A.L., Lawrence, D.M., Seneviratne, S.I., 2020. Warming of hot extremes alleviated by expanding irrigation. Nature Communications 11 (1), 1–7. https://doi.org/10.1038/s41467-019-14075-4.

Thornton, P.E., Thornton, M.M., Mayer, B.W., Wei, Y., Devarakonda, R., Vose, R.S., Cook, R.B., 2018. Daymet: Daily Surface Weather Data on a 1-km Grid for North America, Version 3. ORNL Distributed Active Archive Center. https://doi.org/10.3334/ORNLDAAC/1328.

Tubiello, F.N., Salvatore, M., Golec, Cóndor, Ferrara, A., Rossi, S., Biancalani, R., Flammini, A., 2014. Agriculture , Forestry and Other Land Use Emissions by Sources and Removals by Sinks. FAO - e Food and Agriculture Organization of the United Nations 2, 4–89. Retrieved from. http://www.fao.org/docrep/019/i3671e/i3671e.pdf.

Uddin, J., Hancock, N.H., Smith, R.J., Foley, J.P., 2013. Measurement of evapotranspiration during sprinkler irrigation using a precision energy budget (Bowen ratio, eddy covariance) methodology. Agricultural Water Management 116, 89–100. https://doi.org/10.1016/j.agwat.2012.10.008.

Velpuri, N.M., Senay, G.B., Singh, R.K., Bohms, S., Verdin, J.P., 2013. A comprehensive evaluation of two MODIS evapotranspiration products over the conterminous United States: Using point and gridded FLUXNET and water balance ET. Remote Sensing of Environment 139, 35–49. https://doi.org/10.1016/j.rse.2013.07.013.

World Bank, 2020. Agricultural Land (% of Land Area). World Development Indicators. The World Bank Group, 01-07-. https://data.worldbank.org/indicator/AG.LND.AGRI.ZS. Accessed 01-09-2020.

Wuebbles, D., Hayhoe, K., Kossin, J., Kunkel, K., Stephens, G., Thorne, P., Meteorological Office Richard Somerville, U., 2014. Our Changing Climate. Climate Change Impacts in the United States: The Third National Climate Assessment (2), 19–67. https://doi.org/10.7930/J0KW5CXT.

Xia, Y., Mitchell, K., Ek, M., Sheffield, J., Cosgrove, B., Wood, E., Mocko, D., 2012. Continental-scale water and energy flux analysis and validation for the North American Land Data Assimilation System project phase 2 (NLDAS-2): 1. Intercomparison and application of model products. Journal of Geophysical Research Atmospheres 117 (3). https://doi.org/10.1029/2011JD016048.

Xu, X., Chen, F., Barlage, M., Gochis, D., Miao, S., Shen, S., 2019. Lessons Learned From Modeling Irrigation From Field to Regional Scales. Journal of Advances in Modeling Earth Systems 11 (8), 2428–2448. https://doi.org/10.1029/2018MS001595.

Zhang, Z., Barlage, M., Chen, F., Li, Y., Helgason, W., Xu, X., Li, Z., 2020. Joint Modeling of Crop and Irrigation in the central United States Using the Noah-MP Land Surface Model. Journal of Advances in Modeling Earth Systems 12 (7). https://doi.org/10.1029/2020MS002159.